14th International Conference on Applications of Statistics and Probability in Civil Engineering, ICASP14
Dublin, Ireland, July 9-13, 2023

Workflow-induced uncertainty in probabilistic landslide hazard maps

Anil Yildiz
Postdoctoral researcher, Methods for Model-based Development in Computational Engineering, RWTH Aachen University, Aachen, Germany

Julia Kowalski
Professor, Methods for Model-based Development in Computational Engineering, RWTH Aachen University, Aachen, Germany

ABSTRACT: Increasing complexity and capacity of computational physics-based landslide run-out modelling over the last few years yielded highly efficient model-based decision support tools, e.g. landslide susceptibility or run-out maps, or geohazard risk assessments. Prior to applying such computational models for decision making, however, one has to carefully decide for appropriate and compliant building blocks of the underlying simulation tool chain. For example, one has to decide on resolution and quality of the data products representing topography or vegetation, on the complexity of the underlying process model and on the numerical solution scheme used to solve the process model. Probabilistic hazard mapping based on applied uncertainty quantification (UQ) furthermore requires to decide for model parameter's prior probability distribution, e.g. of friction parameters, as well as how to deal with the UQ-related high-throughput challenge. Surrogate modelling techniques based on Gaussian process emulation reduce the computational costs needed to generate hazard maps while accounting for the error introduced. A comparative study is presented herein by considering a collection of design criteria for a hazard mapping workflow, such as rheological parameters and intensity. Results of multiple model runs for a synthetic case on a real-world topography are illustrated to demonstrate how uncertainty is reflected in hazard maps. Implications regarding the design of model-based decision support tools in practice are discussed.

Quantitative risk analysis (QRA) is crucial in determining areas or elements at risk, and devising strategies on mitigating hazards. Three key factors of a QRA for a natural disaster are hazard, exposure and vulnerability. Exposure and vulnerability characterise assets of societal relevance based on economic, societal, or political metrics. A quantitative assessment of hazard generally requires to understand the hazardous process and is based on empirical, statistical or mechanistic process models. It is composed of the two aspects probability of occurrence and intensity (Corominas et al., 2014). Mapping the hazard in space and time finally requires a combination of temporal and spatial probability of initiation or occurrence, and estimation of run-out, which comprises a spatio-temporal height and velocity field (van Westen et al., 2006).

Risk due to rapid flow-like geohazards such as debris flows can be analysed by calculating the probability of occurrence based on rainfall frequency (Lin et al., 2011), while their intensity is estimated using flow height, flow velocity or a combination of both as proxies (Lateltin et al., 2005; Hürlimann et al., 2008). Lari et al. (2014) links the scarcity of hazard curves for landslides in the literature to the difficulty of generating them, and underlines the importance of selecting an appropriate intensity parameter. For example, Liu et al. (2021) characterises the intensity of a debris flow as high if maximum simulated flow height is between 1.5

and 3.0 m, or if maximum simulated flow height and velocity, i.e. multiplication of both, is between 3.0 and 12.0 m^2/s. Same intensity class is defined by Tang et al. (2022) as maximum flow height more than 2.5 m or maximum flow velocity more than 1.0 m/s.

Regardless the metric used for estimating the intensity of debris flows, a multitude of data products, e.g. Digital Elevation Models (DEM), point clouds, aerial photographs, documented past events (Blahut et al., 2010; Tang et al., 2022), and a computational process model are required to conduct run-out analyses to determine locations of increased risk. Combining these individual building blocks into an integrated workflow facilitates accurate prediction of risk in a model-based decision support tool, e.g. an intensity or a hazard map. It is therefore critical for the development of any model-based decision support tools to design carefully the hazard mapping workflow, hence choosing appropriate decision criteria at each step of the workflow.

Each design decision along the workflow can be understood as a partial model and is hence reflected as an uncertainty in the final hazard map. One can opt for a continuum-mechanical process model, and a decision between a mesh-free, e.g. smoothed particle hydrodynamics, or a structured-mesh, e.g. GIS-based finite difference method, approach can provide considerable differences in the numerical output (Mousavi Tayebi et al., 2021). Given that a GIS-based approach is selected, choosing one digital elevation model (DEM) product over another one can alter the model outcomes (Bühler et al., 2011; Zhao and Kowalski, 2020). Also the method chosen for subsequent uncertainty quantification, e.g. point estimate method vs. Monte Carlo simulations, affect the uncertainty of the parameters used in the post-processed metrics that define the intensity of geohazards (Yildiz et al., 2023). It is therefore essential to learn how to navigate in this *landscape of uncertainties* while conducting geohazard risk assessment, and a holistic attempt to quantify and propagate the accumulated uncertainty subject to each building block of the workflow should be made. Only by considering uncertainties jointly, a reliable frequency distribution of intensities (Lari et al., 2014), and thus a probability distribution can be obtained. Understanding the relative impact of different workflow building blocks on the overall uncertainty, hence reliability of a georisk intensity map will furthermore help to identify *best investments* into increasing the reliability of model-based decision support tools.

An early example of such an attempt is presented herein using debris flows commonly occurring on a catchment in Southern Central Pyrenees in Spain. Run-out simulations with synthetically generated release volumes were conducted to illustrate the uncertainty of an intensity map originating from a collection of decisions in the computational workflow.

1. METHODOLOGY

Workflows to generate probabilistic mapping of various geomorphic hazards, such as earthquake-induced submarine landslides (Collico et al., 2020), landslides on mountainous terrain (Fu et al., 2020), or volcanic hazards (Jones-Ivey et al., 2022), generally present a flowchart demonstrating the data products used, modelling approach, post-processing steps, and methods involved, which obscures the left-out or alternative decisions. Table 1 summarises design options for a landslide risk assessment workflow.

Methodology used in this study consists of a collection of decisions, which can be summarised as follows: i) A GIS-based software which employs finite difference method to solve depth-average shallow flow equations. ii) Model inputs are a digital elevation model file, a release height file, uniformly distributed friction parameters from Voellmy-Salm rheology. iii) Model outputs are maximum flow height and maximum flow velocity iv) Various intensity definitions are compared v) Uncertainty due to friction parameters are assessed in terms of intensity maps.

1.1. Case study

Rebaixader catchment, located near the village Senet in Southern Central Pyrenees in Spain, presents a high torrential activity from a source area with a concave scarp, where debris flows and debris floods initiate. Availability of granular sediment and steep slopes predisposes the basin to tor-

Table 1: Design options for a model-based landslide risk assessment workflow

Decision	**Options**
Modelling approach	*Depth-averaged continuum-mechanics*
	Free-surface continuum-mechanics
	Discrete Particles
	Multi-phase
Numerical approach	*Eulerian*
	Lagrangian
Solution approach	*Analytical*
	Finite element
	Finite difference
	Finite volume
	Smoothed particle hydrodynamics
Rheology	*Voellmy-Salm*
	Bingham
	Herschel–Bulkley
Topography	*Point clouds*
	Digital Elevation Models
	Fine grid vs. Coarse grid
Calibration	*Brute force*
	Grid-type search
	Bayesian inference
Intensity estimation	*Maximum flow height*
	Maximum flow velocity
	Maximum flow height and velocity
	Dynamic pressure
Uncertainty quantification	*Point estimate method*
	Monte Carlo simulations
	First Order Reliability Method
	First Order Second Moment
Prior distributions	*Uniform, Gaussian*
	Beta, Gamma
	Assumed vs. Informed
Emulation strategy	*Gaussian process*

rential flows triggered mainly by rainfall (Oorthuis et al., 2022). An analysis of the relationship between triggering rainfall events and torrential flows showed that short and intense rainstorms in summer triggered flows with a short reaction time between rainfall onset and the initiation of the torrential flows (Abancó et al., 2016). This location is chosen as a case study due to high torrential activity, lack of protective measures, and the availability of long term field monitoring data sets.

1.2. Simulations

A GIS-based open source software framework, r.avaflow v2.4 (Mergili and Pudasaini, 2021), was used in this study to simulate the run-out of a synthetically generated release volume using variable friction coefficients of Voellmy-Salm rheology.

Digital Terrain Model (DTM) and Digital Surface Model (DSM) products of Autonomous body National Center for Geographic Information (CNIG) at 5-m resolution were used in this study (CNIG, 2022). A Canopy Height Model (CHM) was created by subtracting the DTM from DSM, and masking areas with a height difference less than 0.5 m.

A synthetic release height map of ellipsoidal shape with a major axis of 80 m and a minor axis of 30 m was used in this study. Its centre was located at (315645.98, 4712854.18), chosen arbitrarily in the north-facing side of the scarp. Flow height is set to 8 m to yield a flow volume of roughly 15000 m^3 complying with reported debris flows in Oorthuis et al. (2022).

Friction coefficients of Voellmy-Salm rheology are not directly measureable and need to be calibrated based on field observations for a later use in predictive simulations. Friction parameters are used as uncertain parameters varied between simulations scenarios in this study. Dry-Coulomb friction coefficient, μ, was varied between 0.02 and 0.3, while the range of turbulent friction coefficient, ξ, was 100 - 2200 m/s^2 (Zhao et al., 2021; Yildiz et al., 2023).

In order to incorporate the effects of vegetation on the evolution of the flow, a *friction approach* was used that uses modified friction parameters - μ and ξ in case of Voellmy-Salm rheology - in the forest domain to account for the interaction between the debris flow and the forest. This is generally done by increasing μ and reducing ξ (Feistl et al., 2014; Schraml et al., 2015) compared to typical open-terrain values. Friction approach was used in this study by assigning the upper limit to μ ($\mu_f = 0.3$), and the lower limit to ξ ($\xi_f = 100$ m/s^2). These values were considered as static and not changed between simulation scenarios.

Latin Hypercube Sampling was used to sample from input parameter space while maximising the minimum distance between points. A total of 200 input parameter samples were generated yielding a set of 200 simulations with varying friction coefficients. Three stacked raster files, each band corresponding to one simulation results, were used as

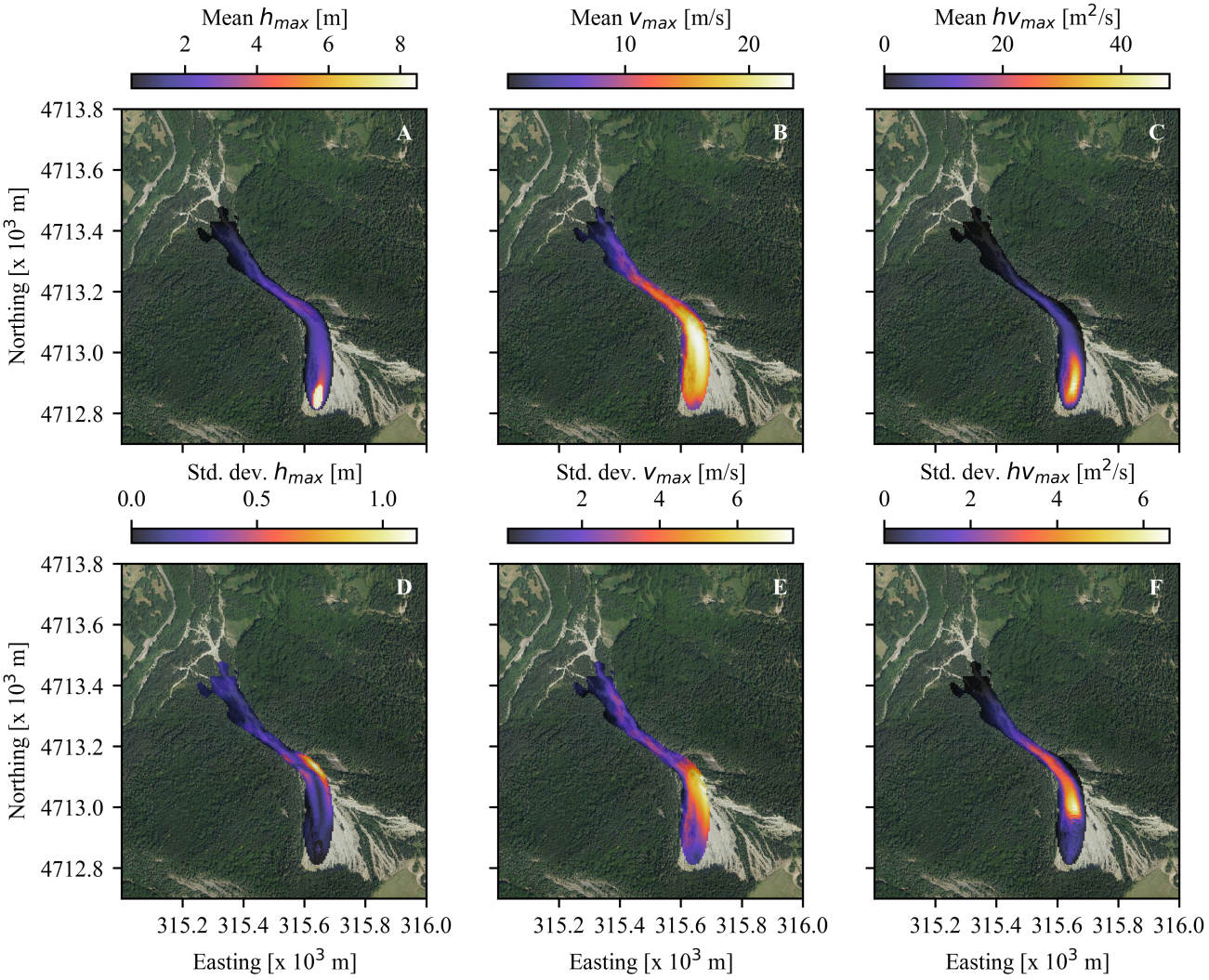

Figure 1: Summaries of the outputs from 200 simulations depicting the (A – C) mean and (D – F) standard deviation of maximum flow height (h_{max}), maximum flow velocity (v_{max}), and maximum flow height x flow velocity (hv_{max}), respectively. Coordinates are given in EPSG:25831.

the main outputs from the model runs. Maximum flow height (h_{max}) and flow velocity (v_{max}) at each cell were auto-generated by r.avaflow 2.4. Two additional outputs were calculated as proxies of maximum discharge and impact pressures (hv_{max} and hv^2_{max}) in each cell. It should be noted that these maxima typically do not occur at the same time step in each cell.

1.3. Hazard assessment

As the hazard is assessed with intensity and probability of an event, a total of 6 criteria from various sources were collected to assess the variation in hazard zoning of the same event based on the definition of intensity. Criteria used in this study can be grouped into three categories: Group 1 combines h_{max} and v_{max}, and consists of Rickenmann (2005) — unpublished source, obtained from Hürlimann et al. (2008) — and Tang et al. (2022). Group 2 combines h_{max} and hv_{max}, and sources are Lin et al. (2011), Chang et al. (2017), and Liu et al. (2021). The last group consists of only Jakob et al. (2012), which uses hv^2_{max}.

2. RESULTS

Figure 1 presents the mean (see Figures 1A – 1C) and standard deviation (see Figures 1D – 1F) of h_{max}, v_{max}, hv_{max} obtained from 200 simulations.

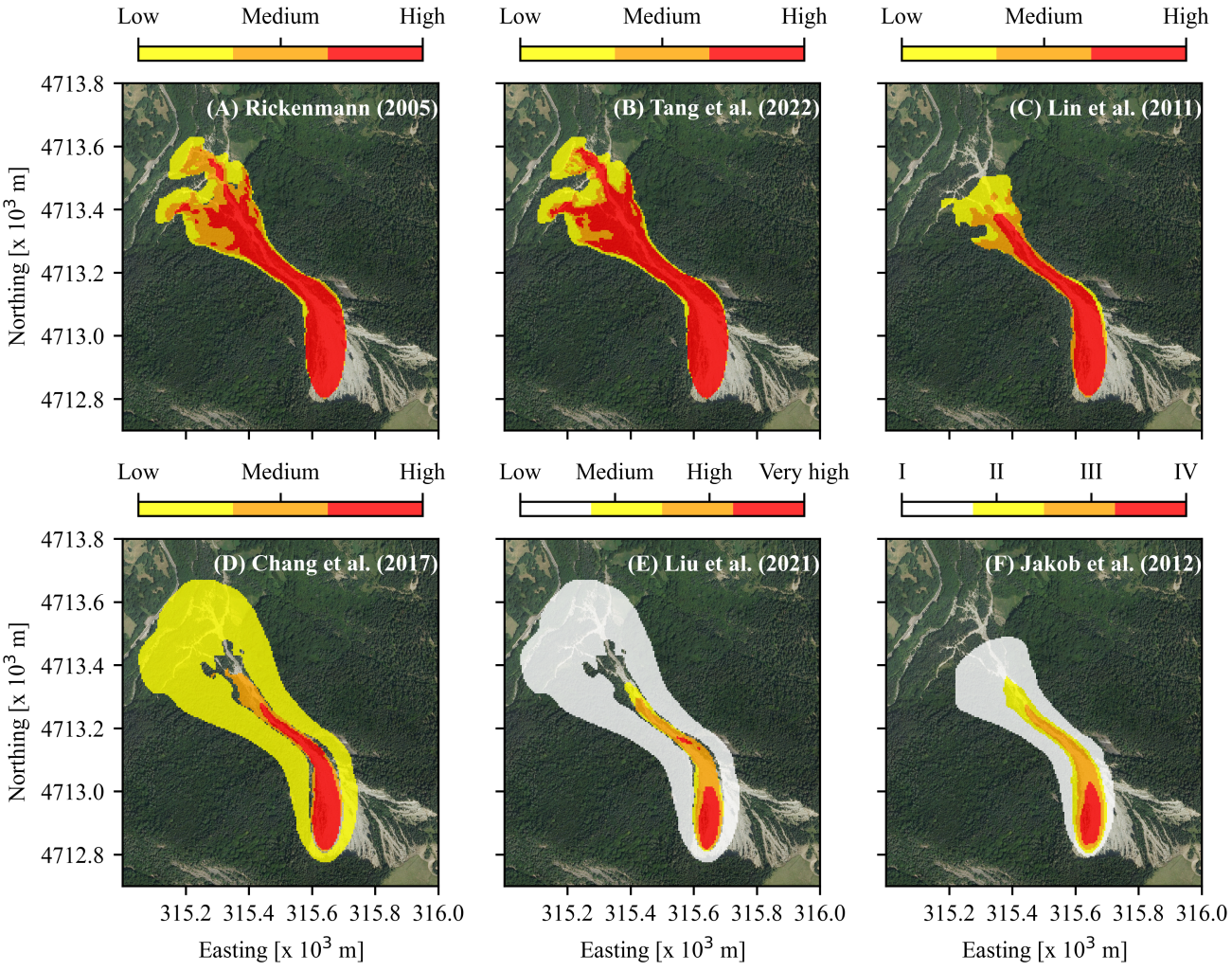

Figure 2: Intensity classes obtained according to (A) Rickenmann (2005), (B) Tang et al. (2022), (C) Lin et al. (2011), (D) Chang et al. (2017), (E) Liu et al. (2021) and (F) Jakob et al. (2012) . Classes are calculated from the mean values from 200 simulations. Coordinates are given in EPSG:25831. Legend in (F) represent complete destruction (IV), major structural damage (III), some structural damage (II), some sedimentation (I).

The flow originates from the synthetically generated location on the upper segment of the north-facing part of the scarp, and follows the channel between the forested area. It reaches the fan at the lower part of the catchment. Flow velocities higher than 20 m/s – mainly at the lower part of the scarp, were obtained from the simulations, which decreased once the flow entered the channel. Higher values of hv_{max} were observed mainly at the lower part of the scarp, which also showed a tendency to decrease as the flow proceeded along the channel.

Highest standard deviation of the flow height was observed at the edges of the channel, with values up to 1 m. Variations from the mean behaviour were of higher magnitude and spatially more distributed for flow velocity. Higher standard deviations at the edges are still evident (See Figure 1E). Unlike h_{max} and v_{max}, highest standard deviations were observed at the lower parts of the scarp and upper parts of the channel for hv_{max}.

Figure 2 illustrates the intensity maps based on the sources mentioned in Section 1.3. Calculations were done using the mean values from 200 simulations. Group 1 — based on h_{max} and v_{max} — marks most of the impacted area as high risk, and

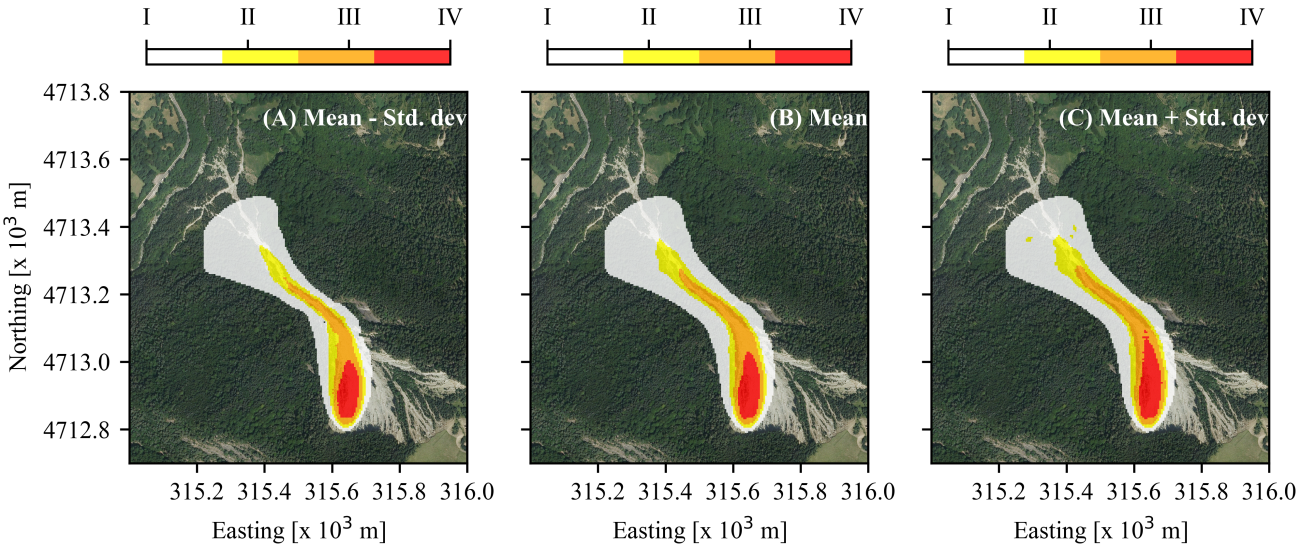

Figure 3: Intensity classes obtained according to Jakob et al. (2012). Classes are calculated from the mean - standard deviation (A), mean (B) and mean + standard deviation (C) from 200 simulations. Coordinates are given in EPSG:25831. Legends represent complete destruction (IV), major structural damage (III), some structural damage (II), some sedimentation (I).

produced highly similar intensity maps with only minor differences (See Figures 2A – 2B). Lin et al. (2011) within Group 2 — based on h_{max} and hv_{max} — produces a smaller area than the others in Group 2, whereas the high intensity areas are similar (See Figures 2C – 2E). Figure 2F shows the intensity classes defined by Jakob et al. (2012), which is only based on hv^2. Classes are defined from I (Some sedimentation) to IV (Complete destruction). Class IV was only marked around the release zone, and the upper parts of the scarp. Channel is marked predominantly as class III (Major structural damage).

Figure 3 show the uncertainty in intensity estimation due to uncertain model parameters. Maps were generated only with Jakob et al. (2012) as an example. Classes were obtained with mean - standard deviation of hv^2_{max} in Figure 3A, with mean hv^2_{max} in Figure 3B, and with mean + standard deviation of hv^2_{max} in Figure 3C. Class IV covers an area of 8325 m^2, 9675 m^2, and 11550 m^2 in Figures 3A, B, and C, respectively.

3. DISCUSSION

Unlike studies of larger scale with spatially and temporally distributed events (Fu et al., 2020; Melo et al., 2018), this study uses a single synthetic flow on a catchment that is highly susceptible to debris flows. Therefore, spatial and temporal probability of the occurrence were not taken into consideration. Uncertainty in the model outputs result from the uncertain rheological parameters, apart from the intrinsic uncertainties due to process idealisation or numerical errors. However, an equal probability can be considered for each simulation as the friction parameters are uniformly distributed.

Highest standard deviations in maximum flow height, hence model-based prediction of least reliability, were observed at the edges of the area transitioning from the scarp to the channel. It can be seen from the orthophotos and from CHM that channel is directly adjacent to the forested area of which the friction parameters are different than the bare earth according to the *friction approach*. Limitations of this approach has been demonstrated for small and medium scale avalanches, and alternatives have been proposed (James Laplante D'Amboise et al., 2022; Védrine et al., 2022). As demonstrated herein with highly uncertain output at the edges of the area impacted by the flow, a risk assessment in a forested area should also investigate alternative methods to incorporate effects of trees on the run-out of geohazards.

A further source of uncertainty as part of the workflow is the choice of intensity metric. Defining intensity of an event and assigning classes to coordinates in a map can be conducted in various ways — all of which requires knowledge about the evolution of the flow in space and time. Selection of parameters and relations are rather unclear (Lari et al., 2014), except (Jakob et al., 2012) which introduces a proxy of dynamic impact pressure validated by data with past events based on the extent and degree of structural damage.

Intensity criteria within each group produced similar maps, especially in Group 1. Lin et al. (2011) has a higher threshold, i.e. 0.2 m, than the others in Group 2, therefore Figure 2C marks the smallest area. Chang et al. (2017) and Liu et al. (2021) produce very similar results even though the latter uses an additional class, *Very high*. Uncertainty generated due to model parameters show that deviations from mean values can affect up to nearly 20% difference in marking high risk zones (See Figure 3).

A significant drawback in some of the intensity definitions used in this study is the use of strict — but not well designed — logical relations, e.g. *and* and *or*, both in Group 1 and 2 can create possible combinations which are left undefined. For example, Chang et al. (2017) defines the low intensity as $0 \leq h < 0.5$ & $vh < 0.5$ and medium intensity as $0.5 \leq h < 2.5$ & $0.5 \leq vh < 2.5$. Areas with an h between 0.5 and 2.5 and a vh less than 0.5 are undefined in this case. Figures 2D and 2E illustrate the unclassified areas between the medium and low classes. The spatial coverage of such areas was rather small in this specific case study, but this may lead to significant errors in judgement for other cases.

4. CONCLUSIONS

This study demonstrates an example of how the uncertainty due to workflow used in generating a model-based risk assessment for geohazards affects the final output. It was demonstrated that employing a well-established intensity criteria is crucial, as the poorly described criteria can alter the decision-making process of risk zoning. Future research will focus on demonstrating the uncertainty at each step, and how it is propagated through the workflow and reflected in the final output, e.g. a probabilistic hazard map.

ACKNOWLEDGEMENTS

The authors would like to extend their gratitude to Marcel Hürlimann (UPC Barcelona) and Claudia Abanco (Universitat de Barcelona) for the fruitful discussions on Rebaixader catchment.

5. REFERENCES

Abancó, C., Hürlimann, M., Moya, J., and Berenguer, M. (2016). "Critical rainfall conditions for the initiation of torrential flows. Results from the Rebaixader catchment (Central Pyrenees)." *Journal of Hydrology*, 541, 218–229.

Blahut, J., Horton, P., Sterlacchini, S., and Jaboyedoff, M. (2010). "Debris flow hazard modelling on medium scale: Valtellina di Tirano, Italy." *Natural Hazards and Earth System Sciences*, 10(11), 2379–2390.

Bühler, Y., Christen, M., Kowalski, J., and Bartelt, P. (2011). "Sensitivity of snow avalanche simulations to digital elevation model quality and resolution." *Annals of Glaciology*, 52(58), 72–80.

Chang, M., Tang, C., Van Asch, T. W. J., and Cai, F. (2017). "Hazard assessment of debris flows in the Wenchuan earthquake-stricken area, South West China." *Landslides*, 14(5), 1783–1792.

CNIG (2022). "Centro de Descargas del Organismo Autónomo Centro Nacional de Información Geográfica, <https://centrodedescargas.cnig.es>.

Collico, S., Arroyo, M., Urgeles, R., Gràcia, E., Devincenzi, M., and Peréz, N. (2020). "Probabilistic mapping of earthquake-induced submarine landslide susceptibility in the South-West Iberian margin." *Marine Geology*, 429, 106296.

Corominas, J., van Westen, C., Frattini, P., Cascini, L., Malet, J.-P., Fotopoulou, S., Catani, F., Van Den Eeckhaut, M., Mavrouli, O., Agliardi, F., Pitilakis, K., Winter, M. G., Pastor, M., Ferlisi, S., Tofani, V., Hervás, J., and Smith, J. T. (2014). "Recommendations for the quantitative analysis of landslide risk." *Bulletin of Engineering Geology and the Environment*, 73, 209–263.

Feistl, T., Bebi, P., Teich, M., Bühler, Y., Christen, M., Thuro, K., and Bartelt, P. (2014). "Observations and modeling of the braking effect of forests on small and

medium avalanches." *Journal of Glaciology*, 60(219), 124–138.

Fu, S., Chen, L., Woldai, T., Yin, K., Gui, L., Li, D., Du, J., Zhou, C., Xu, Y., and Lian, Z. (2020). "Landslide hazard probability and risk assessment at the community level: a case of western Hubei, China." *Natural Hazards and Earth System Sciences*, 20(2), 581–601.

Hürlimann, M., Rickenmann, D., Medina, V., and Bateman, A. (2008). "Evaluation of approaches to calculate debris-flow parameters for hazard assessment." *Engineering Geology*, 102(3-4), 152–163.

Jakob, M., Stein, D., and Ulmi, M. (2012). "Vulnerability of buildings to debris flow impact." *Natural Hazards*, 60(2), 241–261.

James Laplante D'Amboise, C., Teich, M., Hormes, A., Steger, S., and Berger, F. (2022). "Modeling Protective Forests for Gravitational Natural Hazards and How It Relates to Risk-Based Decision Support Tools." *Protective Forests as Ecosystem-based Solution for Disaster Risk Reduction (Eco-DRR)*, M. Teich, C. Accastello, F. Perzl, and K. Kleemayr, eds., IntechOpen.

Jones-Ivey, R., Patra, A., and Bursik, M. (2022). "Workflows for Construction of Spatio-Temporal Probabilistic Maps for Volcanic Hazard Assessment." *Frontiers in Earth Science*, 9, 744655.

Lari, S., Frattini, P., and Crosta, G. (2014). "A probabilistic approach for landslide hazard analysis." *Engineering Geology*, 182, 3–14.

Lateltin, O., Haemmig, C., Raetzo, H., and Bonnard, C. (2005). "Landslide risk management in Switzerland." *Landslides*, 2(4), 313–320.

Lin, J.-Y., Yang, M.-D., Lin, B.-R., and Lin, P.-S. (2011). "Risk assessment of debris flows in Songhe Stream, Taiwan." *Engineering Geology*, 123(1), 100–112.

Liu, B., Hu, X., Ma, G., He, K., Wu, M., and Liu, D. (2021). "Back calculation and hazard prediction of a debris flow in Wenchuan meizoseismal area, China." *Bulletin of Engineering Geology and the Environment*, 80(4), 3457–3474.

Melo, R., van Asch, T., and Zêzere, J. L. (2018). "Debris flow run-out simulation and analysis using a dynamic model." *Natural Hazards and Earth System Sciences*, 18(2), 555–570.

Mergili, M. and Pudasaini, S. P. (2014-2021). "r.avaflow - The mass flow simulation tool, <https://www.avaflow.org>.

Mousavi Tayebi, S. A., Moussavi Tayyebi, S., and Pastor, M. (2021). "Depth-Integrated Two-Phase Modeling of Two Real Cases: A Comparison between r.avaflow and GeoFlow-SPH Codes." *Applied Sciences*, 11(12), 5751.

Oorthuis, R., Hürlimann, M., Vaunat, J., Moya, J., and Lloret, A. (2022). "Monitoring the role of soil hydrologic conditions and rainfall for the triggering of torrential flows in the Rebaixader catchment (Central Pyrenees, Spain)." *Landslides*.

Schraml, K., Thomschitz, B., McArdell, B. W., Graf, C., and Kaitna, R. (2015). "Modeling debris-flow runout patterns on two alpine fans with different dynamic simulation models." *Natural Hazards and Earth System Sciences*, 15(7), 1483–1492.

Tang, Y., Guo, Z., Wu, L., Hong, B., Feng, W., Su, X., Li, Z., and Zhu, Y. (2022). "Assessing Debris Flow Risk at a Catchment Scale for an Economic Decision Based on the LiDAR DEM and Numerical Simulation." *Front. Earth Sci. Sec. Geohazards and Georisks*, 10, 821735.

van Westen, C., van Asch, T., and Soeters, R. (2006). "Landslide hazard and risk zonation—why is it still so difficult?." *Bulletin of Engineering Geology and the Environment*, 65(2), 167–184.

Védrine, L., Li, X., and Gaume, J. (2022). "Detrainment and braking of snow avalanches interacting with forests." *Natural Hazards and Earth System Sciences*, 22(3), 1015–1028.

Yildiz, A., Zhao, H., and Kowalski, J. (2023). "Computationally-feasible uncertainty quantification in model-based landslide risk assessment." *Frontiers in Earth Science*, 10, 1032438.

Zhao, H., Amann, F., and Kowalski, J. (2021). "Emulator-based global sensitivity analysis for flow-like landslide run-out models." *Landslides*, 18(10), 3299–3314.

Zhao, H. and Kowalski, J. (2020). "Topographic uncertainty quantification for flow-like landslide models via stochastic simulations." *Natural Hazards and Earth System Sciences*, 20(5), 1441–1461.